Seasonal and topographic variations in porewaters of a southeastern USA salt marsh as revealed by voltammetric profiling†

David C. Bull and Martial Taillefert*

School of Earth and Atmospheric Sciences, Georgia Institute of Technology, Atlanta, GA 30332-0340, USA. E-mail: mtaillef@eas.gatech.edu; Fax: +1 (404) 894 5638; Tel: +1 404 894 6043

Received 19th September 2001, Accepted 23rd October 2001
Published on the Web 1st November 2001

Article

We report electrochemical profiles from unvegetated surficial sediments of a Georgia salt marsh. In creek bank sediments, the absence of ΣH_2S or FeS_{aq} and the presence of Fe(III)–organic complexes suggest that Mn and Fe reduction dominates over at least the top *ca.* 5 cm of the sediment column, consistent with other recent results. In unvegetated flats, accumulation of ΣH_2S indicates that SO_4^{2-} reduction dominates over the same depth. A summer release of dissolved organic species from the dominant tall form *Spartina alterniflora*, together with elevated temperatures, appears to result in increased SO_4^{2-} reduction intensity and hence high summer concentrations of ΣH_2S in flat sediments. However, increased bioturbation and/or bioirrigation seem to prevent this from happening in bank sediments. Studies of biogeochemical processes in salt marshes need to take such spatial and temporal variations into account if we are to develop a good understanding of these highly productive ecosystems. Furthermore, multidimensional analyses are necessary to obtain adequate quantitative pictures of such heterogeneous sediments.

Introduction

Much of the Atlantic coast of North America is bordered by salt marshes dominated by *Spartina* spp. grasses. These marshes are extremely productive environments exhibiting rapid geochemical cycling.[1] Factors such as tidal regime, temperature, topography, hydrology, vegetation, infauna and microbiota[1–4] act in concert to produce a geochemically complex environment. Chemical studies of both spatial and seasonal variations are few.[1,5–7] Recent studies of salt marshes[8–12] have employed voltammetric sensors for their high spatial resolution, ability to sample sediment porewaters with minimal physical or chemical disturbance, and ability to simultaneously measure several important dissolved analytes including O_2, Mn^{2+}, Fe^{2+}, iron(III)–organic complexes $Fe^{III}L$, soluble FeS species, and reduced sulfur species ΣH_2S ($= S^{2-} + HS^- + H_2S + S^0 + S_x^{2-}$).[8,11–15] In this paper, we attempt to illustrate, and account for, chemical differences between surficial sediment porewaters (upper *ca.* 5 cm) from two types of local environment, and changes over a period of several months.

Bioturbated marine sediments are highly heterogeneous, and sources and sinks for porewater analytes can be highly localised. Consequently, in 1D representations where lateral fluxes are neglected, it is easy to overestimate vertical transport processes such as fluxes at the sediment/water interface.[16] One-dimensional approaches generally limit our ability to account for complex features of sediments. Several studies have obtained 2D views of marine sediments by careful sectioning (*e.g.* ref. 17), by the diffusive gradients in thin films (DGT) technique (*e.g.*ref. 18) or by image analysis.[19] Using voltammetric microelectrodes, Luther *et al.*[20] have compiled separate 1D profiles into a 3D representation of sediment porewaters surrounding a worm burrow. Here, we employ arrays of voltammetric electrodes, lowered together into the sediment at well-defined positions and scanned sequentially, to construct temporally and spatially synchronised 3D profiles of sediment porewaters for the first time. This constitutes a further step toward adequate portrayals of these complex systems.

The study site

The Saltmarsh Ecosystem Research Facility (SERF) at the Skidaway Institute of Oceanography on Skidaway Island, Georgia, southeastern USA, was the location for this study. This is a 600′ boardwalk out into intertidal, regularly inundated, tall *Spartina alterniflora* marsh. Two distinct unvegetated environments were sampled; flats between *Spartina* plots and soft, muddy creek banks. Crab, worm, and shrimp burrows were observed throughout the site, but were substantially more numerous on creek banks. Temperatures increased considerably during the study; mean air temperatures in the nearby city of Savannah varied from 11.1 °C in February and 15.0 °C in March to 26.1 °C in June and 27.8 °C in July (NOAA). Sea surface temperatures off the Savannah coast followed a very similar trend (NOAA).

Methods

On four occasions—February, March, June and July—8 cm in diameter × at least 20 cm deep cores were taken from within 30′ of the boardwalk during falling tides. Sediments were only cored while submerged, and the overlying water was retained throughout sampling and analysis.

High resolution voltammetric profiling, using Au|Hg microelectrode probes, was carried out essentially as described previously.[8,21] Profiles were always obtained some centimetres from obvious burrow openings. For the March cores and the June flat core, four or five working electrodes were bundled together and scanned sequentially at each depth using a DLK-MUX-1 electrode multiplexer (Analytical Instrument Systems, Inc.: AIS); electrode tips were no closer than 6 mm in the horizontal plane, and no further apart than 42 mm. For the February and March cores, a combination pH microelectrode

†Presented during the ACS Division of Geochemistry symposium 'Biogeochemical Consequences of Dynamic Interactions Between Benthic Fauna, Microbes and Aquatic Sediments', San Diego, April 2001.

DOI: 10.1039/b108493c

(Diamond General Development Corp.) was similarly positioned next to the working electrode(s). For the July cores, a DLK-MAN-1 micromanipulator (minimal depth increment 0.1 mm) and controller (AIS), were substituted for the manual micromanipulator (Narishige) used otherwise. The working electrode used in the June flat core, and two of those used in the July flat core (Fig. 7 and 8), were steel-housed probes constructed from surgical stainless steel capillary tubing and Teflon-coated 75 μm in diameter gold wire (A-M Systems); total tip diameters were approximately 0.5 mm. Allowing for the smaller electrode diameter, sensitivities for these electrodes were similar to those for glass-bodied electrodes, and voltammograms for the two types of electrodes were indistinguishable.

Voltammetric peak and wave heights and potentials were extracted from scan files using a linear background subtraction procedure. Where necessary, overlapping peaks were deconvoluted into two Gaussian curves, using Peakfit v. 4 (Jandel Scientific Software). The electrodes were calibrated against O_2 and Mn^{2+} standards before use, and the pilot ion method[8] was used to quantify Fe^{2+} and ΣH_2S. Sensitivities are not yet available for $Fe^{III}L$ and FeS_{aq}, and hence these analytes are reported as peak currents rather than concentrations.

Results from bundled electrodes are represented as arrays of coloured polygons. Each polygon shows analyte concentrations at a given depth below the sediment/water interface (SWI). The polygons are arranged in order of increasing depth, reading from the left to the right of the figure, and then from top to bottom. The vertices indicate the coordinates of the working electrodes, and the position of the pH electrode (when present) is marked with an $\times$. Spectral hue indicates concentration of the analyte; colouring within the polygon is calculated by linear interpolation of the concentrations observed at each electrode at that depth.

Results

With the onset of summer the marsh changed markedly. Extensive new growth of *Spartina* was observed, and thin coatings of brown algae formed on creek banks. Fiddler crab population and activity were observed to increase dramatically, leaving creek banks riddled with burrows. Throughout the sampling period, bank sediments were mostly brownish, while flat sediments were dark, low-saturation colours.

Bank sediments

In the February bank core profile (Fig. 1), O_2 was detected down to 0.5 mm below the SWI. The pH decreased from the SWI down to a shallow minimum of 6.47 at *ca.* 5 mm. Mn^{2+} appeared at 9 mm and slowly increased to *ca.* 30 μm at a depth of 51 mm. It was joined by Fe^{2+} at 16 mm, also steadily increasing to a maximum of 108 μm. A peak assigned to $Fe^{III}L$, $E_p \approx -0.4$ V, appeared at 45 mm. Below 51 mm, Mn^{2+} and Fe^{2+} tailed off, while the $Fe^{III}L$ signal increased to *ca.* 75 nA.

In March, only Fe^{2+} was observed (Fig. 2), with considerable local heterogeneity. This core was taken from a point at which the creek bank sloped steeply, so the SWI and the Fe^{2+} polygons were sharply inclined. (In Fig. 2, the slope is roughly parallel to the plotted *y*-axis, so the designated origin is also the lowest point in each polygon.) (1) The largest Fe^{2+} source is near the surface around the designated origin, seen as a broad profile beginning immediately below the SWI, reaching 318 μm at 6 mm and disappearing around 20 mm. At the other electrodes, respectively clockwise; (2) *ca.* 50 μm between 20 and 30 mm below SWI, then (3) only *ca.* 30 μm between 10 and 13 mm below SWI, and (4) a narrow feature, maximum 144 μm, between 6 and 9 mm below SWI, and a second, maximum 38 μm, between 36 and 42 mm. The initial decrease in pH was marked, from *ca.* 7.6 in the overlying waters to 7.22

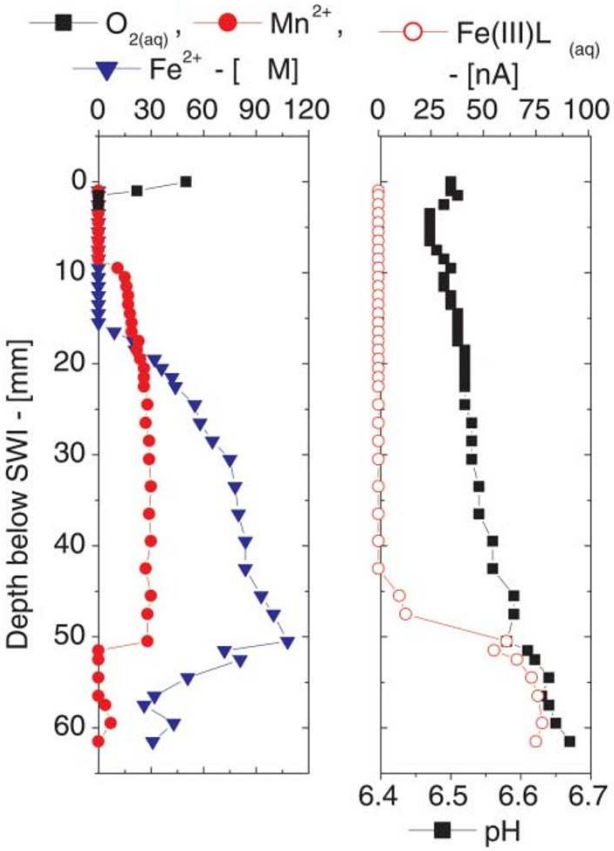

Fig. 1 Voltammetric and pH profiles, bank core, February.

at the SWI to *ca.* 6.7 below 8 mm. There was no subsequent increase with depth in this case.

In June, O_2 was only detected above the SWI (Fig. 3). Porewater Mn^{2+} appeared immediately at the SWI, and by 7 mm had reached a stable concentration of about 450 μm. Below 34 mm it was abruptly replaced by Fe^{2+}, which reached a maximum of 870 μm at 37 mm, then disappeared by 51 mm. It was replaced in turn by $Fe^{III}L$, first seen at 44 mm, reaching a maximum of 55 nA at 58 mm, and tailing off at the bottom of the profile, 74 mm.

In the July bank core (Fig. 4), Mn^{2+} was observed out into the overlying water, taking a maximum of 111 μm at 10 mm below SWI, and persisting underneath the Fe^{2+} maximum of 336 μm at 35 mm. As the profile ends at 39 mm, it is not possible to see whether $Fe^{III}L$ is still present below *ca.* 4 cm, as in the June core (Fig. 3).

'Flat' sediments

The February flat core (Fig. 5) closely resembled the February bank core, although concentration maxima were somewhat greater and shallower throughout. The pH was 6.59 at the SWI, decreased to a minimum of 6.51 at *ca.* 4 mm, then steadily underwent a marked increase with depth, to a final value of 6.87. O_2 was not observed below the SWI. Mn^{2+} and Fe^{2+} were first seen just below the SWI, increasing gradually with depth to maxima of 135 μm for Mn^{2+} at 36 mm, 741 μm for Fe^{2+} at 40 mm. $Fe^{III}L$ appeared at 20 mm, and again currents became more intense with the disappearance of Mn, reaching a record 150 nA at the bottom of the profile.

ΣH_2S dominated the March flat core (Fig. 6), though traces of other analytes were occasionally visible. It was first observed around 12 mm below the SWI on all five electrodes, and reached concentrations near the bottom of the profile of 560, 16, 114, 506, and 460 μm, respectively, clockwise from the designated origin, indicating a 'front' of sulfide diffusing both upward and in the *y*-direction. O_2 was only detected above the

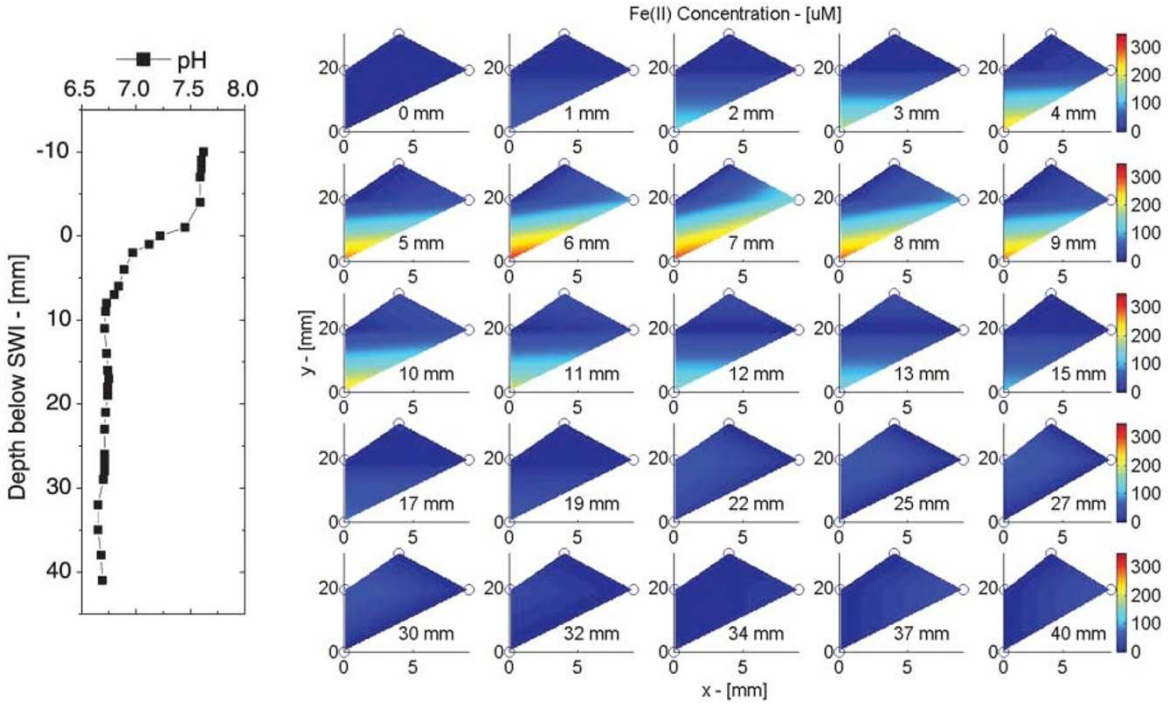

Fig. 2 pH profile (left) and Fe^{2+} distribution in 3D (right), bank core, March; pH electrode coordinates (−7, 3).

SWI. The pH was 6.81 at the SWI, decreasing to a minimum of 6.20 at 20 mm, then recovering to 6.3 by 45 mm, the bottom of the profile.

In June, again O_2 was not observed in the sediment (Fig. 7), and again ΣH_2S dominated the core at depth; it was first detected 9 mm below the SWI, and reached 1680 µm at the bottom of the profile. However, large signals were also evident for other species. $Fe^{III}L$ appeared at 3 mm depth, Fe^{2+} at 4 mm, Mn^{2+} and FeS_{aq} at 9 mm. $Fe^{III}L$, Fe^{2+} and Mn^{2+} shared a maximum at 11 mm below SWI, of 50 nA, 1630 µm and 1310 µm, respectively. Mn^{2+} and $Fe^{III}L$ abruptly disappeared at 15 mm, but Fe^{2+} and FeS_{aq} persisted down to 24 mm, with a second Fe^{2+} maximum at 19 mm.

ΣH_2S in July (Fig. 8) began at *ca.* 8 mm below the SWI on all four electrodes. Again, there is an apparent 'front', moving upward and laterally from the peak value of 2290 µm at the bottom of the profile, in the upper left corner of the polygon. FeS_{aq} was often observed below *ca.* 5 mm on all electrodes, reaching current intensities around 20 nA, and disappearing as ΣH_2S increased over *ca.* 500 µm. Fe^{2+} was briefly observed just below the SWI at the designated origin, reaching 110 µm at 4 mm depth before abruptly disappearing. O_2 did not penetrate into the sediment.

Discussion

Sedimentary heterotrophic microorganisms may use inorganic electron acceptors such as O_2, NO_3^-, MnO_2, FeOOH or SO_4^{2-}

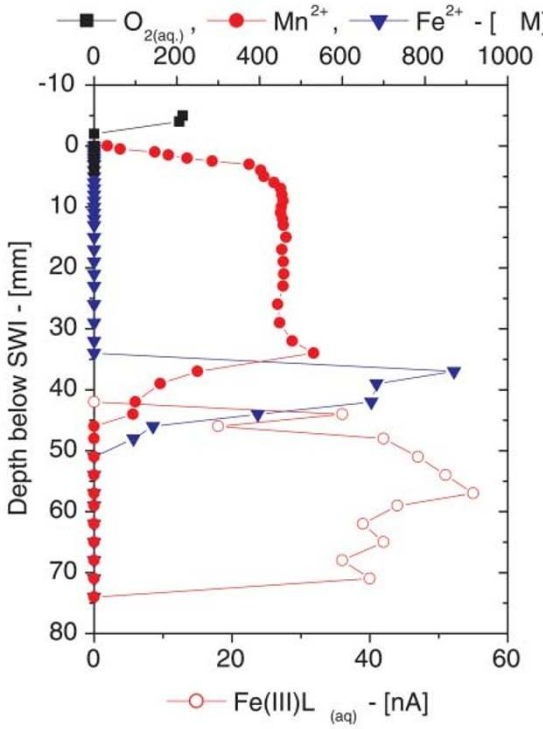

Fig. 3 Voltammetric profile, bank core, June.

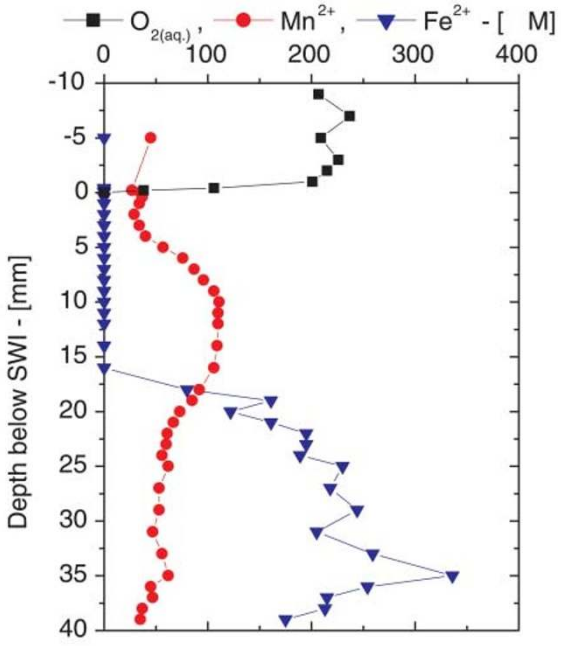

Fig. 4 Voltammetric profile, bank core, July.

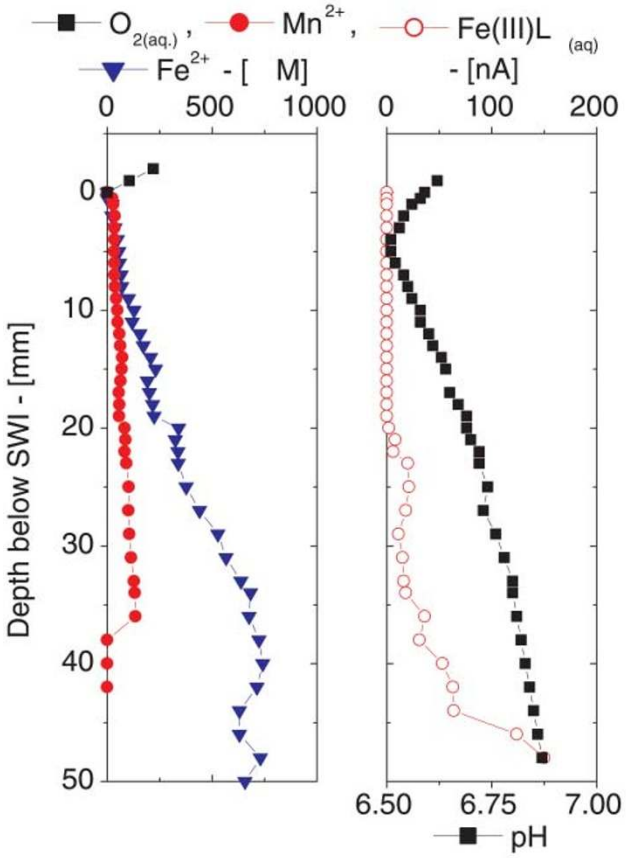

Fig. 5 Voltammetric and pH profiles, flat core, February.

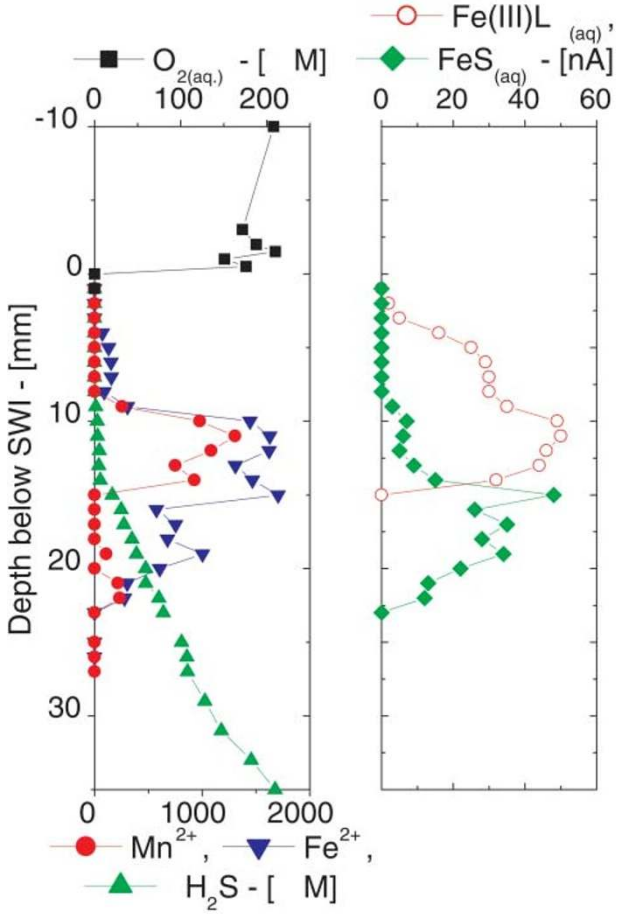

Fig. 7 Voltammetric profiles, flat core, June.

to oxidise organic carbon (*e.g.* ref. 22), resulting in redox stratification. Conventionally, oxidants yielding more negative ΔG^0 should be consumed preferentially, *i.e.*, in the order $O_2 > NO_3^- \sim MnO_2 > FeOOH > SO_4^{2-}$.[22] These species themselves (O_2), their reduced forms (Mn^{2+}, Fe^{2+}, H_2S), or subsequent products (S_x^{2-}, S_0, FeS_{aq}, and $S_2O_3^{2-}$) can be detected voltammetrically,[8,11–15] and we were also able to observe concomitant pH changes whenever the pH electrode

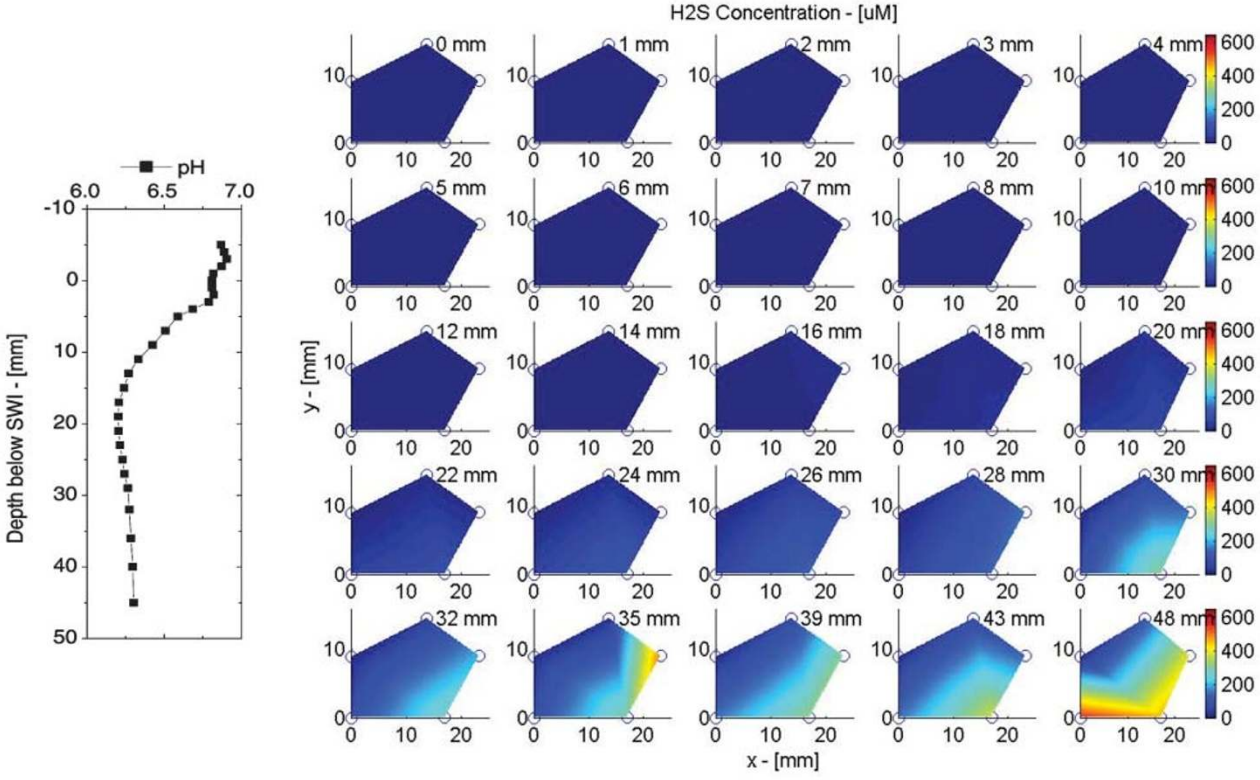

Fig. 6 pH profile (left) and ΣH_2S distribution in 3D (right), flat core, March; pH electrode coordinates (6, −4).

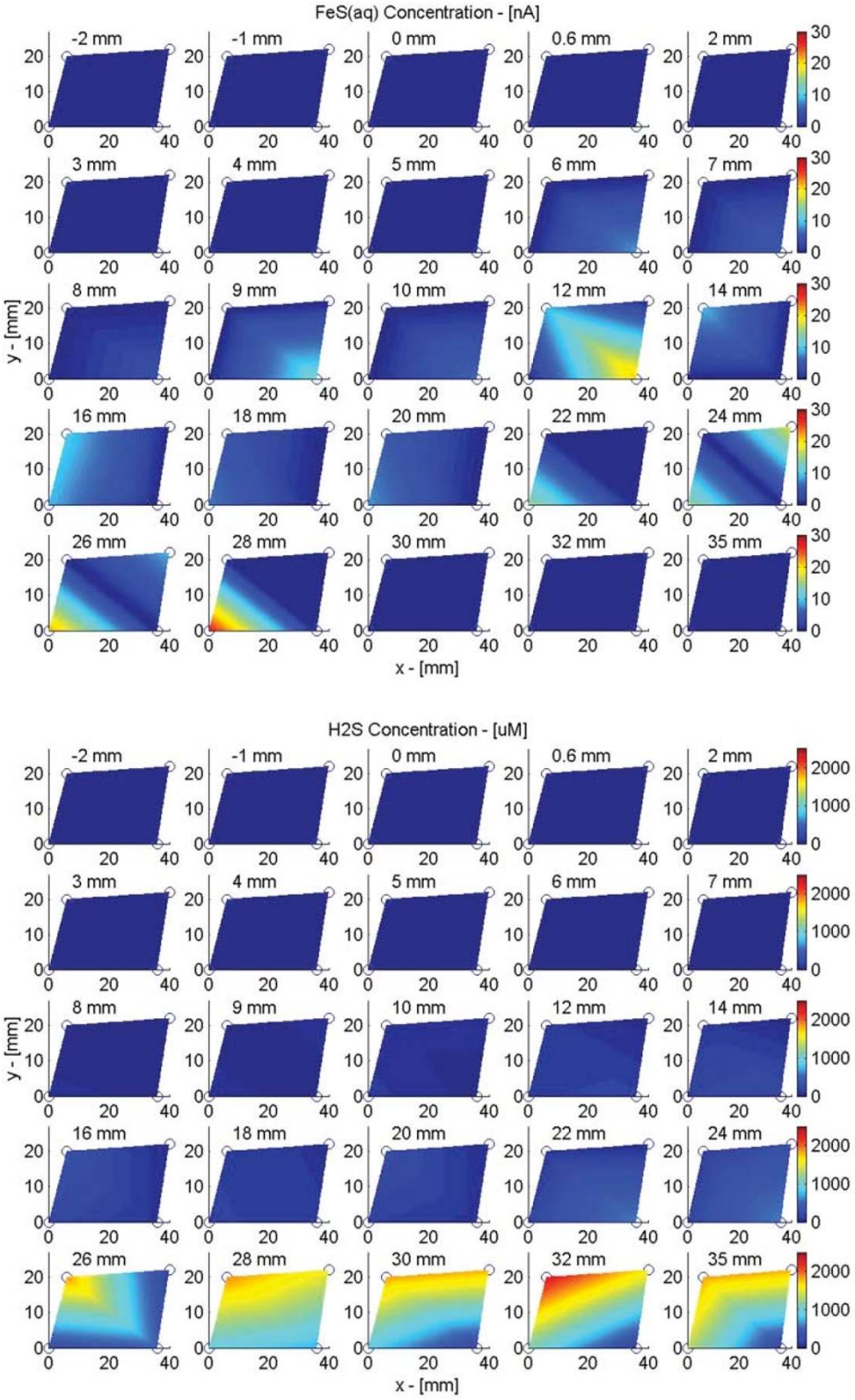

Fig. 8 3D distributions of FeS_{aq} (above), and ΣH_2S (below), flat core, July.

was deployed. Thus, these chemical profiles of porewaters shed light on chemical and microbiological processes operating in the sediment.

H_2S can undergo a number of abiotic side reactions with other major redox species (Table 1). This includes the reduction of MnO_2 to Mn^{2+}, FeOOH to Fe^{2+}, and the reduction of $Fe^{III}L$ (Eq. 3), which is particularly rapid.[15] Precipitation with Fe^{2+} seems to occur *via* a detectable intermediate, FeS_{aq} (eqn. (4)). Abiotic reoxidation by O_2 regenerates MnO_2, FeOOH, and SO_4^{2-}, completing the redox cycles (Table 2).

pH profiles in the February and March bank cores (Fig. 1 and 2), and in the February flat core (Fig. 5), are typical of organic matter-rich coastal sediments.[9,30] The pH decrease in the first *ca.* 5 mm is ascribed to H^+-producing O_2 and NO_3^- oxidation of organic carbon. Subsequent increase with depth is ascribed to H^+-consuming reduction of Mn and Fe oxides,

Table 1 Some important side reactions of H_2S in early diagenesis[a]

(1)	$MnO_2 + H_2S + 2H^+ \rightarrow Mn^{2+} + S^0 + 2H_2O$
(2)	$2FeOOH + H_2S + 4H^+ \rightarrow 2Fe^{2+} + S^0 + 4H_2O$
(3)	$2FeL_n^{3-2n} + H_2S + nH^+ \rightarrow 2Fe^{2+} + S^0 + nHL^{-b}$
(4)	$Fe^{2+} + H_2S \xrightarrow{-2H^+} FeS_{aq} \rightarrow FeS_s$

[a]*e.g.*ref. 14, 15, 22–24. [b]L is assumed to be a bidentate oxygen donor ligand, and *n* is the number of such ligands in the complex.

Table 2 Selected reoxidation reactions[a]

(5)	$2Mn^{2+} + O_2 + 2H_2O \rightarrow 2MnO_2 + 4H^+$
(6)	$4Fe^{2+} + O_2 + 6H_2O \rightarrow 4FeOOH + 8H^+$
(7)	$4FeS + 9O_2 + 6H_2O \rightarrow 4FeOOH + 4SO_4^{2-} + 8H^{2+}$
(8)	$H_2S + 2O_2 \rightarrow SO_4^{2-} + 2H^+$

[a]*e.g.*ref. 25–29.

confirmed here by the appearance of Mn^{2+} and then Fe^{2+}. The thermodynamic sequence[22] of O_2 disappearance followed by the appearance of Mn^{2+}, Fe^{2+} was observed in the other bank cores (Fig. 2–4), at successively shallower depth—indeed, in July Mn^{2+} had diffused out into the overlying water.

Heterotrophic SO_4^{2-} reduction initially yields H_2S; but neither H_2S, nor the partially reoxidised forms S_x^{2-}, S_0, or $S_2O_3^{2-}$, were ever detected in the first 40–80 mm of any of the bank cores (Fig. 1–4). Nor was FeS_{aq}, which would be generated in the presence of such high levels of Fe^{2+}.[14] Also, sulfides rapidly reduce $Fe^{III}L$ (eqn. (3)) yet $Fe^{III}L$ was seen in the February and June bank cores (Fig. 1 and 3). These observations suggest that SO_4^{2-} reduction is not an important mechanism in these surficial sediments. Thus, sulfide reduction of MnO_2 and FeOOH (eqn. (1) and eqn. (2)) is unlikely to be significant over the depth profiled, and the principal reduction mechanisms for these minerals appear to be biological.

While this suggestion runs counter to the prevailing view that SO_4^{2-} reduction is the principal electron-accepting process in salt marshes, at least in vegetated sediments,[31,32] similar results have recently been obtained in the nearby Sapelo Island salt marsh. Lowe *et al.*[4] found that iron-reducing bacteria were most abundant in the top 6 cm of a core from an unvegetated creek bank, whereas SO_4^{2-}-reducing bacteria were most abundant in deeper sediments. Porewater SO_4^{2-} did not decrease significantly from SWI levels until around 6 cm depth. Both observations suggest that Fe and Mn reduction dominates in surficial sediments. Kostka *et al.*[33] reported Fe reduction rates approximately 4 times greater than SO_4^{2-} reduction rates in the upper 5 cm of unvegetated creek banks; although they suggested that abiotic reaction with sulfide species accounted for some of the Fe reduction, on the basis that the sum of Fe and SO_4^{2-} rates substantially exceeded their measured carbon mineralisation rate. In a subsequent paper,[34] they used geochemical parameters, rate measurements and bacterial counts to conclude that Fe reduction was the predominant microbial respiration process in either bioturbated or vegetated sediments at their study site.

Sulfide accumulation

While the February flat core (Fig. 5) most closely resembled the February bank core (Fig. 1), extensive porewater ΣH_2S accumulation, and hence SO_4^{2-} reduction, were observed in the March flat core (Fig. 6). The deeper pH minimum, around 20 mm below the SWI, may be due to H^+-producing reoxidation of H_2S or FeS.[30]

The June flat core (Fig. 7) was also mostly sulfidic, with ΣH_2S reaching 2 mM. High concentrations of Fe^{2+} led to formation of FeS_{aq} and presumably precipitation of FeS_s (eqn. (4)); between 15 and 22 mm, FeS_s was theoretically supersaturated unless the pH was $\leqslant 5$. $Fe^{III}L$ was observed above 15 mm, and since it rapidly reacts with H_2S to form Fe^{2+} and S^0 (eqn. (3)), ΣH_2S was most probably dominated by S^0 above 15 mm. Nonetheless, H_2S was rapidly supplied to the upper core by diffusion along the steep ΣH_2S concentration gradient from the bottom of the profile, allowing ready abiotic reduction of reactive Fe and Mn (eqn. (1)–(3)), and possibly accounting for much of the observed Fe^{2+} and Mn^{2+}.

Observed ΣH_2S concentrations in 'flat' sediments increased dramatically during the study period, and cores became sulfidic at a shallower and shallower depth (Fig. 5–8). The same trend has previously been reported for New Hampshire salt marshes, and ascribed to the release of significant amounts of dissolved organic carbon by tall form *Spartina alterniflora* during the summer growth period.[1,35] This release, combined with elevated summer temperatures, greatly increases SO_4^{2-} reduction rates, as SO_4^{2-} reduction in marine sediments is organic matter-limited and temperature-dependent.[36,37] Here, H_2S accumulation appeared to begin in March (Fig. 6), somewhat earlier than in the more temperate New Hampshire climate.[1]

The role of bioturbation

We propose that the dichotomy between largely suboxic bank sediments and largely sulfidic flat sediments is due to the more extensive bioturbation inferred in creek banks (*cf.*ref. 33, 34, 38). This ensures a strong supply of O_2, and freshly formed MnO_2 and FeOOH, all probably more reducible than SO_4^{2-}.[22] Not only does this disfavour H_2S production, but these oxidants will also reactively consume any H_2S that is formed (eqn. (1)–(3) and (8)).

There are several distinct supply mechanisms: bioturbation by crabs and other infauna mixes well-oxidised material down the sediment column,[2,39] providing a deep reservoir of Fe and Mn oxides, and of Fe–organic complexes. Furthermore, in well-worked sediments, MnO_2 and FeOOH contents are broadly dependent on particle surface area.[40] Consequently, the finer bank sediments can be expected to contain more reactive Fe and Mn, and hence have an inherently greater poising capacity. Conversely, burrowing and deposit feeding bring reduced sediments and associated porewaters up to the surface, directly exposing them to well oxygenated water or to air.[39,41] This substantially enhances O_2 reoxidation of subsurface reduced species (eqn. (5)–(8)), particularly Fe^{2+} for which oxidation is rapid.[25] Bioirrigation also supplies O_2 to the deep sediment, both through the actions of occupying macrofauna[42,43] and passively by flow of oxygenated water through burrows.[44-46] Further, on the sloping banks, burrows can drain fully, and subsequent drying allows air into burrows and cracks.

Since fiddler crab population (*cf.* ref. 47) and activity (*cf.* ref. 48) appeared to increase substantially during the sampling period, bioturbation and bioirrigation should have increased substantially, too.[2] Polychaete worms may also make a significant contribution to sediment oxidation, even when burrowing crab population is high[19] and polychaete density would also be expected to increase in late spring.[49] Thus, even in summer conditions favouring SO_4^{2-} reduction, bioturbation and bioirrigation were able to provide sufficient O_2 and reactive Mn and Fe oxides to keep bank sediments suboxic to the 40–80 mm limit of profiling depth.

Formation of iron (III)–organic complexes

Soluble iron(III)–organic complexes have been detected electrochemically[8,11] or by other techniques[6,50] in salt marsh sediments on a few previous occasions. $Fe^{III}L$ was a significant feature of four of the eight core profiles given here (Fig. 1, 3, 5, 7). Taillefert *et al.*[21] have collated several mechanisms for formation of $Fe^{III}L$ in marine sediments (Table 3):

In this study, $Fe^{III}L$ only occurred at depth, so O_2 or

Table 3 $Fe^{III}L$ formation processes

(9)	$4FeL_n^{2-2n} + O_2 + 4H^+ \rightarrow 4FeL_n^{3-2n} + 2H_2O$
(10)	$10Fe^{2+} + 2NO_3^- \xrightarrow{\text{bacteria, HL}^-} 10FeL_n^{3-2n} + N_2$
(11)	$2Fe^{2+} + MnO_2 \xrightarrow{HL^-} 2FeL_n^{3-2n} + Mn^{2+}$
(12)	$FeOOH + Fe^*L_n^{2-2n} \rightarrow Fe^{2+} + Fe^*L_n^{3-2na}$
(13)	$FeOOH + nHL^- + (4-n)H^+ \rightarrow FeL_n^{3-2n} + 2H_2O$

[a]The star label is added to track the reactive pathway of that iron atom.

bacterially mediated NO_3^- (ref. 51) oxidation of $Fe^{II}L$ complexes (eqn. (9) and (10)) seem unlikely formation mechanisms. The $Fe^{III}L$ current intensity was generally inversely correlated with Mn^{2+}, indicating that Mn oxidation of $Fe^{II}L$ complexes (eqn. (11)) was not a significant formation mechanism in this case, either. Furthermore, oxygen-donor ligand-mediated electron transfer from FeOOH (eqn. (12)) is slow above pH 6,[52,53] while the pH was always above 6 in the February and March cores, and presumably also in the equally suboxic June bank core (Fig. 3). Thus nonreductive dissolution of FeOOH (eqn. (13)) was most likely the principal mechanism of $Fe^{III}L$ formation in these cores. However, it is not clear why the $Fe^{III}L$ current intensity maxima were also deeper than the Fe^{2+} concentration maxima (Fig. 1, 3 and 5), *i.e.* at a depth where a significant proportion of FeOOH had already been consumed. We hypothesize that $Fe^{III}L$ was still produced above that depth, but efficiently removed by metal-reducing bacteria which were able to utilise it as an electron acceptor.

Sediment heterogeneity

We note that concentrations in plane differ widely from electrode to electrode in the 3D profiles (Fig. 2, 6 and 8) as might be expected in a heterogeneous sediment. The ΣH_2S profiles of the March and July flat cores (Fig. 6 and 8) suggest a 'front' diffusing obliquely upward from deeper sediments. However, the March bank Fe^{2+} (Fig. 2) and July flat FeS_{aq} profiles (Fig. 8) show patchier profiles which may reflect microbial or chemical niches. Nonetheless, in each array similar vertical trends are seen at each electrode, and therefore we believe that single profiles are still qualitatively representative of their immediate environment. Thus, while it may be possible to identify the processes occurring in a sediment on the basis of a 1D profile, a quantitative understanding appears to require 3D representation. We strongly recommend increased use of multidimensional techniques, especially in bioturbated sediments such as those studied here, which exhibit significant heterogeneity.

Conclusion

We report electrochemical profiles from unvegetated surficial sediments of a Georgia salt marsh. In creek bank sediments, the absence of ΣH_2S or FeS_{aq} and the presence of Fe(III)–organic complexes indicate that Mn and Fe reduction dominates over at least the top *ca.* 5 cm of the sediment column, consistent with other recent results. In unvegetated flats, accumulation of ΣH_2S indicates that SO_4^{2-} reduction dominates over the same depth, as the product ΣH_2S is observed. A summer release of dissolved organic species from the dominant tall form *Spartina alterniflora*, together with elevated temperatures, appears to result in increased SO_4^{2-} reduction intensity and hence high summer concentrations of ΣH_2S in flat sediments. However, increased bioturbation and/or bioirrigation seem to prevent this from happening in bank sediments. Studies of biogeochemical processes in salt marshes need to take such spatial and temporal variations into account if we are to develop a good understanding of these highly productive ecosystems. Furthermore, multidimensional analyses are necessary to obtain adequate quantitative pictures of such heterogeneous sediments.

This study is part of ongoing attempts to characterise the chemistry of southeastern USA salt marshes. Future studies will examine the solid phase speciation and size distribution, the microbial population, the nature and extent of bioturbation, the biogeochemistry around sediment features such as burrows, and modelling early diagenesis, in these sediments and in other local environments of the salt marsh.

Acknowledgements

Acknowledgement is made to the Donors of The Petroleum Research Fund, administered by the American Chemical Society, for partial support of the Symposium of the ACS that gave rise to this special issue. Field trips were funded by Georgia Tech's FRP in Marine Science and Technology. Laboratory facilities at Skidaway Institute of Oceanography were very kindly provided by Dr Rick Jahnke. Matt Snyder assisted with sampling and laboratory work. We thank Dr Carolyn Ruppel and Greg Schultz for some helpful discussions. Drs Wei-Jun Cai and Joel Kostka generously provided copies of their papers in press. Two anonymous referees supplied detailed and thoughtful reviews.

References

1 M. E. Hines, S. L. Knollmeyer and J. B. Tugel, *Limnol. Oceanogr.*, 1989, **34**, 578–590.
2 L. C. Katz, *Est. Coastal Mar. Sci.*, 1980, **11**, 233–237.
3 J. E. Kostka and G. W. Luther, III, *Biogeochemistry*, 1995, **29**, 159–181.
4 K. L. Lowe, T. J. DiChristina, A. N. Roychoudhury and P. Van Cappellen, *Geomicrobiol. J.*, 2000, **17**, 163–178.
5 M. C. Morrison and M. E. Hines, *Atmos. Environ.*, 1990, **24**, 1771–1779.
6 G. W. Luther, III, T. G. Ferdelman, J. E. Kostka, E. J. Tsamakis and T. M. Church, *Biogeochemistry*, 1991, **14**, 57–88.
7 D. T. Osgood and J. C. Zieman, *Estuaries*, 1998, **21**, 767–783.
8 P. J. Brendel and G. W. Luther, III, *Environ. Sci. Technol.*, 1995, **29**, 751–761.
9 W. J. Cai, P. Zhao, S. M. Theberge, A. Witter, Y. Wang and G. W. Luther III, in *Environmental Electrochemistry: Analyses of Trace Element Biogeochemistry*, ed. M. Taillefert and T. F. Rozan, ACS Symposium Series, Washington, DC, vol. 811, 2001, pp. 188–209.
10 B. T. Glazer, S. C. Cary, L. Hohmann and G. W. Luther, III, in *Environmental Electrochemistry: Analyses of Trace Element Biogeochemistry*, ed. M. Taillefert and T. F. Rozan, ACS Symposium Series, Washington, DC, vol. 811, 2001, pp. 283–305.
11 G. W. Luther, III, B. T. Glazer, L. Hohmann, J. I. Popp, M. Taillefert, T. F. Rozan, P. J. Brendel, S. M. Theberge and D. B. Nuzzio, *J. Environ. Monit.*, 2001, **3**, 61–66.
12 M. Taillefert, V. C. Hover, T. F. Rozan, S. M. Theberge and G. W. Luther, III, *Estuaries*, submitted.
13 M. Taillefert, G. W. Luther, III and D. B. Nuzzio, *Electroanalysis*, 2000, **12**, 401–412.
14 S. M. Theberge and G. W. Luther III, *Aquat. Geochem.*, 1997, **3**, 191–211.
15 M. Taillefert, A. B. Bono and G. W. Luther III, *Environ. Sci. Technol.*, 2000, **34**, 2169–2177.
16 M. P. Harper, W. Davison and W. Tych, *Environ. Sci. Technol.*, 1999, **33**, 2611–2616.
17 M. Huettel, W. Ziebis, S. Forster and G. W. Luther, III, *Geochim. Cosmochim. Acta*, 1998, **62**, 613–631.
18 S. M. Shuttleworth, W. Davison and J. Hamilton-Taylor, *Environ. Sci. Technol.*, 1999, **33**, 4169–4175.
19 D. C. Bull and R. B. Williamson, *Environ. Sci. Technol.*, 2001, **35**, 1658–1662.
20 G. W. Luther, III, P. J. Brendel, B. L. Lewis, B. Sundby, L. Lefrancois, N. Silverberg and D. B. Nuzzio, *Limnol. Oceanogr.*, 1998, **43**, 325–333.
21 M. Taillefert, T. F. Rozan, B. T. Glazer, J. Herszage, R. E. Trouwborst and G. W. Luther, III, in *Environmental Electrochemistry: Analyses of Trace Element Biogeochemistry*, ed. M. Taillefert and T. F. Rozan, ACS Symposium Series, Washington, DC, vol. 811, 2001, pp. 247–264.
22 P. N. Frölich, G. P. Klinkhammer, M. L. Bender, N. A. Luedtke,

G. R. Heath, D. Cullen and P. Dauphin, *Geochim. Cosmochim. Acta*, 1979, **43**, 1075–1090.
23 C. R. Myers and K. H. Nealson, *Geochim. Cosmochim. Acta*, 1988, **52**, 2727–2732.
24 A. J. Pyzik and S. E. Sommer, *Geochim. Cosmochim. Acta*, 1981, **45**, 687–698.
25 W. Sung and J. J. Morgan, *Environ. Sci. Technol.*, 1980, **14**, 561–568.
26 W. Stumm and J. J. Morgan, in *Aquatic Chemistry: Chemical Equilibria and Rates in Natural Waters*, Wiley, New York, 1996, pp. 683–686.
27 D. M. Di Toro, J. D. Mahony and A. M. Gonzales, *Environ. Toxicol. Chem.*, 1996, **15**, 2156–2167.
28 F. J. Millero, S. Hubinger, M. Fernandez and S. Garnett, *Environ. Sci. Technol.*, 1987, **21**, 439–443.
29 H. L. Ehrlich, *Earth-Sci. Rev.*, 1996, **45**, 45–60.
30 P. Van Cappellen and Y. Wang, *Am. J. Sci.*, 1996, **296**, 197–243.
31 R. W. Howarth, in *Aquatic Microbiology: An Ecological Approach*, ed. T. E. Ford, Blackwell Scientific Publications, Cambridge, MA, 1993.
32 D. M. Alongi, *Coastal Ecosystem Processes*, CRC Press, NY, 1998.
33 J. E. Kostka, A. Roychoudhury and P. Van Cappellen, *Biogeochemistry*, in press.
34 J. E. Kostka, B. Gribsholt, E. Petrie, D. Dalton, H. Skelton and E. Kristensen, *Limnol. Oceanogr.*, in press.
35 M. E. Hines, R. S. Evans, B. R. Sharak Genthner, S. G. Willis, S. Friedman, J. N. Rooney-Varga and R. Devereux, *Appl. Environ. Microbiol.*, 1999, **65**, 2209–2216.
36 R. A. Berner and J. T. Westrich, *Am. J. Sci.*, 1985, **285**, 193–206.
37 J. T. Westrich and R. A. Berner, *Geomicrobiol. J.*, 1988, **6**, 99–117.
38 B. Thamdrup, in *Advances in Microbial Ecology*, ed. B. Schink, Kluwer Academic Publishers, New York, vol. 16, 2000.
39 R. B. Williamson, R. J. Wilcock, B. E. Wise and S. E. Pickmere, *Environ. Toxicol. Chem.*, 1999, **18**, 2078–2086.
40 S. N. Luoma, in *Heavy metals in the marine environment*, ed. R. W. Furness and P. S. Rainbow, CRC Press, Boca Raton, Florida, 1990, pp. 51–66.
41 N. P. Revsbech, J. Sørensen, T. H. Blackburn and J. P. Lomholt, *Limnol. Oceanogr.*, 1980, **25**, 403–411.
42 P. S. Meadows and J. Tait, *Mar. Biol.*, 1989, **101**, 75–82.
43 R. L. Marinelli and B. P. Boudreau, *J. Mar. Res.*, 1996, **54**, 939–966.
44 J. W. Harvey, R. M. Chambers and J. R. Hoelscher, *Estuaries*, 1995, **18**, 568–578.
45 P. V. Ridd, *Est. Coastal Shelf Sci.*, 1996, **43**, 617–625.
46 C. E. Hughes, P. Binning and G. R. Willgoose, *J. Hydrol.*, 1998, **211**, 34–49.
47 J. M. Teal, *Ecology*, 1962, **43**, 614–624.
48 G. N. Knopf, *Crustaceana*, 1966, **11**, 302–306.
49 R. Sarda, K. Foreman and I. Valiela, *Mar. Biol.*, 1995, **121**, 431–445.
50 G. W. Luther, III, P. A. Shellenbarger and P. J. Brendel, *Geochim. Cosmochim. Acta*, 1996, **60**, 951–960.
51 K. L. Straub and B. E. E. Buchholz-Cleven, *Appl. Environ. Microbiol.*, 1998, **64**, 4846–4856.
52 D. Suter, S. Banwart and W. Stumm, *Langmuir*, 1991, **7**, 809–813.
53 G. W. Luther, III, J. E. Kostka, T. M. Church, B. Sulzberger and W. Stumm, *Mar. Chem.*, 1992, **40**, 81–103.